Quasisteady space-charge fields in photorefractive multiple quantum wells: Edge effects

María Aguilar,* M. Carrascosa, and F. Agulló-López
Departamento de Física de Materiales, Universidad Autónoma de Madrid, 28049 Madrid, Spain

L. Solymar
Department of Engineering Science, University of Oxford, Parks Road, Oxford OX1 3PJ, United Kingdom

L. F. Magaña
Instituto de Física, Universidad Nacional Autónoma de México, 20364 México Distrito Federal, Mexico
(Received 26 June 1996; revised manuscript received 26 September 1996)

An analytical solution has been obtained for the quasi-steady-state space-charge fields recorded in a photoconductive multiple quantum well (MQW) neglecting longitudinal mobility. The results apply to times longer than the transverse but shorter than the longitudinal relaxation time. The finite thickness of the structure has been explicitly taken into account by using a two-dimensional formulation, i.e., including parallel and perpendicular components for the field. The analysis refers to parallel geometry and has been applied to two different physical situations: (a) electron-hole generation from interband transitions and (b) electron generation from suitable donors. This latter case has been summarily discussed for comparison purposes. The longitudinal profiles for the trap densities as well as for the two components of the space-charge field have been determined. They show relevant edge effects that depend inversely on the ratio of dielectric constants in the MQW and buffer layers. The role of some relevant parameters such as grating period and applied field on these effects has been investigated. Finally, the results have been compared with the short-time solution and with previous works using a one-dimensional approach. [S0163-1829(97)00108-2]

I. INTRODUCTION

Recently, much attention is being devoted to the photorefractive effect in thin slabs such as semiconductor multiple quantum wells[1,2] (MQW) and polymer films.[3,4] They are very promising candidates for a number of applications such as spatial light modulators, optical correlators, real time holography, or ultrafast spectroscopy.[5–9] For those thin-film structures, the one-dimensional formulation[10] generally used to describe the generation of a light-induced space-charge field pattern in bulk materials may not be appropriate although it has been applied to describe MQW performance.[11,12] In fact, when the film thickness is comparable or smaller than the grating period, edge effects associated to the slab faces may become relevant. Therefore, a two-dimensional approach including both parallel and perpendicular components of fields and currents appears to be necessary. MQW structures are particularly interesting in this respect as they typically involve an active thickness of ~ 1 μm. Since this value is of the order or even smaller than possible light-grating periods, relevant edge effects may appear. Two configurations have been used in experimental work depending on the direction of the applied field. In the transverse geometry, the field is parallel to the quantum well planes and the dominating electro-optic effect is the exciton lifetime broadening. In the longitudinal geometry, the field is perpendicular to the quantum wells therefore selecting the quantum confined Stark effect as the leading electro-optic mechanism. The transverse geometry shares much in common with traditional bulk photorefractive materials because the applied electric field is parallel to the grating vector and transport is essentially along the quantum well planes. In contrast, in the longitudinal configuration the grating vector is perpendicular to the applied field and the transport mechanisms are more complex. In this geometry, several authors have dealt with cross-well transport,[13–16] as well as with the grating dynamics.[17]

First two-dimensional analyses for thin-film structures operating in both parallel[18] and perpendicular geometries[19,20] have been reported. Unfortunately, only the short-time solution was obtained in those works. Some marked differences with regard to the one-dimensional solution, including edge effects were predicted. However, charge screening should operate during the overall recording process and may presumably reduce or even eliminate some of the two-dimensional effects. Therefore, in order to achieve a more complete and useful description of the photorefractive performance, one would require the full time-dependent solution. This will provide a more realistic assessment of the features obtained with the two-dimensional formulation. Although an analytical solution has been obtained for an isotropic slab[21] the extension to an anisotropic film is not available.

The purpose of this paper is to offer an analytical solution for the light-induced steady-state charge field generated in MQW where perpendicular (longitudinal) transport has been neglected and operating in the parallel geometry. This is an ideal situation but may approximately represent the operation of a MQW with a very long transport time through the structure (low perpendicular mobility) as often found in practice. In this case there is a quasi-steady-state for times larger than the parallel relaxation time but shorter than the perpendicular relaxation time. For very long times perpendicular fields are screened out and so edge effects disappear. In this paper we

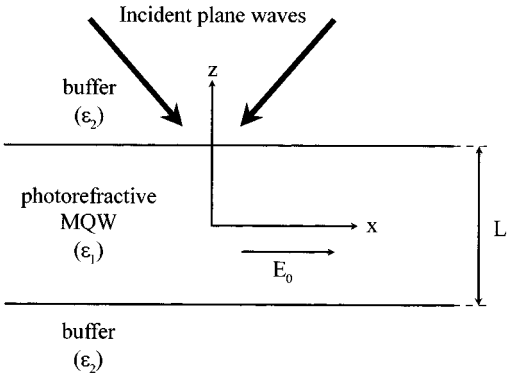

FIG. 1. Schematic diagram of the experimental geometry.

will deal with this intermediate quasisteady situation. Moreover, in order to facilitate the mathematical analysis, light attenuation has also been ignored. This restriction is not a serious shortcoming in many practical cases and it may be removed in future work. Two different physical situations have been considered in our work. In one, electrons and holes are created through interband transitions. This is the situation found in the reported experimental work.[2] The other one considers that either electrons or holes are generated by photoionization of suitable deep donors. (e.g., Cr in GaAs/$Al_xGa_{1-x}As$ MQW). This is a simpler case from the point of view of mathematics and has been discussed for comparison purposes. In both situations the carriers are trapped in deep defects acting as acceptors, and the MQW structure has to be semi-insulating to minimize the dark current. The dependence of the generated space-charge fields on some geometrical and physical parameters has been worked out and discussed in comparison to the short-time solution and the one-dimensional approaches.

II. PHYSICAL MODEL FOR A PHOTOREFRACTIVE MQW

Our theoretical analysis will refer to a MQW illuminated by a sinusoidal light intensity pattern in a parallel geometry as schematically depicted in Fig. 1. In the more general case, the MQW structure is sandwiched between two dielectric (not photoconductive) buffer layers. Very often, the upper layer is removed. Carriers are supposed to be generated by the two processes illustrated in Figs. 2(a) and 2(b) and corresponding to two different physical situations. In Fig. 2(a) both electrons and holes are created from interband transitions and then are rapidly trapped at discrete levels in the wells. This is the situation generally used in experiments. For simplicity a single level well will be assumed and the electron population in the continuum levels will be neglected. In Fig. 2(b) electrons (a similar process would apply to holes) are created by transitions from donor levels into the continuum states of the conduction band. Although this case cannot be easily implemented in practice and so no experimental information is available, it helps to establish the universality of the edge effects with independence of the specific physical model. It will be assumed in both cases that photoionized carriers can move in the parallel (x,y) plane with a high mobility whereas perpendicular transport (along

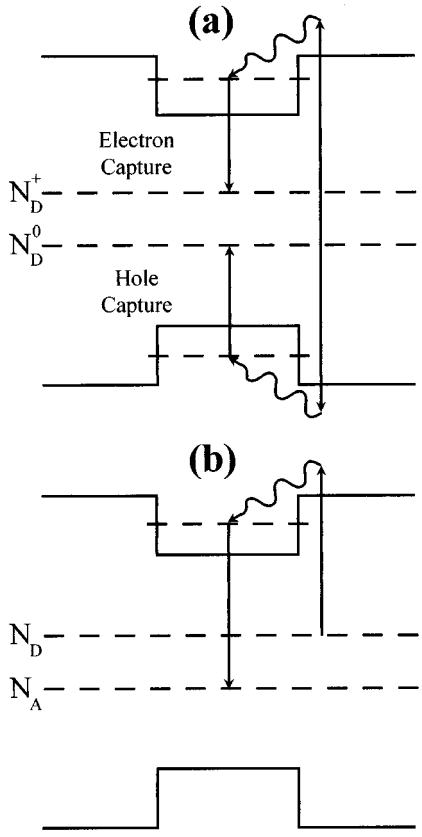

FIG. 2. Carrier transition processes in a photorefractive quantum well structure with (a) interband transitions and (b) electron transitions from donor levels.

z) is neglected ($\mu_z=0$). This is an ideal situation but is necessary to avoid the complicating features of carrier trapping at the MQW boundaries or buffer layers. Moreover, it may represent a reasonable approximation in many practical cases where effective mobilities μ_z are much lower than μ_x.[13] Under this condition, a quasisteady solution has been worked out that applies to recording times that are longer than the transverse relaxation time $\tau_T=\epsilon\epsilon_0/I\alpha\tau n\mu_x$ but shorter than the longitudinal relaxation time $\tau_L=\epsilon\epsilon_0/I\alpha\tau n\mu_z$. For very long times ($t>\tau_L$), the perpendicular mobility allows longitudinal transport and therefore edge effects will be screened out in times of the order of seconds. Another simplifying feature of our model is to ignore the dark photoconductivity, i.e., we consider the MQW to be perfectly insulating (it only has to be semi-insulating). Although these approximations may appear as drastic simplifications of the real physical problem, we expect that they will show the key features of the edge effects derived from the two-dimensional formulation.

In Secs. III and V we will consider the equations that govern the photoionization and trapping processes in the MQW for the situations in Figs. 2(a) and 2(b), respectively.

III. CARRIER GENERATION FROM INTERBAND TRANSITIONS

A. Equations for the recording process

The physical situation used in experiments corresponds to Fig. 2(a). The equations include electron and hole transport

and band to band photoexcitation. Using the notation for MQW structures proposed by Nolte and Melloch,[2] the equations governing the recording process are

$$\frac{\partial n_e}{\partial t}=\frac{\alpha}{h\nu}I-\gamma n_e N_D^+ +\frac{1}{e}\vec{\nabla}\cdot\vec{J}_e\,, \tag{1a}$$

$$\frac{\partial n_h}{\partial t}=\frac{\alpha}{h\nu}I-\gamma n_h N_D^0 -\frac{1}{e}\vec{\nabla}\cdot\vec{J}_h\,, \tag{1b}$$

$$\frac{\partial N_D^+}{\partial t}=-\frac{\partial N_D^0}{\partial t}=-\gamma n_e N_D^+ +\gamma n_h N_D^0\,, \tag{1c}$$

$$\frac{\partial E_x}{\partial x}+\frac{\partial E_z}{\partial z}=\frac{\rho}{\epsilon\epsilon_0}, \tag{1d}$$

$$\frac{\partial E_x}{\partial z}-\frac{\partial E_z}{\partial x}=0, \tag{1e}$$

with

$$\rho=e(N_D^+-N_A^-), \tag{1f}$$

$$\vec{J}_e=e\mu_e n_e\vec{E}+e\mathcal{D}_e\vec{\nabla}n_e\,, \tag{1g}$$

$$\vec{J}_h=e\mu_h n_h\vec{E}-e\mathcal{D}_h\vec{\nabla}n_h\,, \tag{1h}$$

where n is the carrier concentration, $\vec{J}$ is the current, ρ is the charge density, $\vec{E}$ is the electric field, α is the absorption coefficient for the active interband transition (attenuation has been however neglected since the condition $\alpha L\ll 1$ is assumed), γ is the recombination coefficient, μ is the transverse mobility, and $\mathcal{D}$ is the diffusion coefficient which is related to μ through $\mathcal{D}=k_BT\mu/e$. In all these cases, the subindexes e and h refer to electrons and holes, respectively. The equations consider that electron-hole recombination takes place at the trap centers whose concentration is designated as N_D^+ for electrons and N_D^0 for holes. $N_A^-=N_D^+(0)$ is the density of shallow acceptors which assure the crystal's neutrality. Thermal excitation of carriers and direct recombination is neglected. These traps are usually introduced by proton implantation or low temperature growth. Our physical model assumes $j_z=0$ and so the current densities (j_e for electrons and j_h for holes) refer to the x component.

For the steady state the above Eqs. (1) become

$$\frac{\alpha}{h\nu}I-\gamma_e n_e N_D^+ +\frac{1}{e}\vec{\nabla}\cdot\vec{J}_e=0, \tag{2a}$$

$$\frac{\alpha}{h\nu}I-\gamma_h n_h N_D^0 -\frac{1}{e}\vec{\nabla}\cdot\vec{J}_h=0, \tag{2b}$$

$$-\gamma_e n_e N_D^+ +\gamma_h n_h N_D^0=0, \tag{2c}$$

$$\frac{\partial E_x}{\partial x}+\frac{\partial E_z}{\partial z}=\frac{\rho}{\epsilon\epsilon_0}, \tag{2d}$$

$$\frac{\partial E_x}{\partial z}-\frac{\partial E_z}{\partial x}=0. \tag{2e}$$

It has been further assumed, for simplicity that $N_{D0}^+=N_A^-=N/2$, and $\gamma_e=\gamma_h=\gamma$, which markedly simplifies the mathematics without harming the physics.

Under sinusoidal intensity illumination, $I=I_0(1+m\,\mathrm{Re}[e^{iKx}])$, one proposes for all the magnitudes in Eq. (2) a solution of the form

$$n_{e,h}=n_{e,h\,0}+\mathrm{Re}[n_{e,h\,1}e^{iKx}], \tag{3a}$$

$$N_D^+=N_{D0}^+ +\mathrm{Re}[N_{D1}^+e^{iKx}], \tag{3b}$$

$$E_x=E_0+\mathrm{Re}[E_{x1}e^{iKx}], \tag{3c}$$

$$E_z=\mathrm{Re}[E_{z1}e^{iKx}], \tag{3d}$$

including the average and modulated components for all magnitudes. With the above assumptions and $m\ll 1$ to allow for linearization one obtains after substitution of (3) into (2),

$$n_{e0}=n_{h0}=n, \tag{4}$$

and

$$N_{D1}^+=\frac{N_r}{n}(n_{h1}-n_{e1}), \tag{5}$$

where

$$n_{e1}=\frac{2mE_{me}(E_D+iE_0)+iE_{x1}(E_{me}+E_{mh}+E_D+iE_0)}{E_{me}(E_D+iE_0)+E_{mh}(E_D-iE_0)+E_D^2+E_0^2}, \tag{6a}$$

$$n_{h1}=\frac{2mE_{mh}(E_D+iE_0)-iE_{x1}(E_{me}+E_{mh}+E_D-iE_0)}{E_{me}(E_D+iE_0)+E_{mh}(E_D-iE_0)+E_D^2+E_0^2}, \tag{6b}$$

with $E_D=Kk_BT/e$ and $E_{me,h}=\gamma N_r/\mu_{e,h}K$ being characteristic fields and N_r is an effective trap concentration given by $N_r=N_A^-N_D^+/(N_A^-+N_D^+)=N/4$.

Further algebraic manipulations lead to the differential equation

$$\frac{\partial^2E_{x1}}{\partial z^2}-\Gamma_{\mathrm{eh}}^2E_{x1}-imK^2E_qA=0, \tag{7}$$

where

$$\Gamma_{\mathrm{eh}}^2=K^2(1+B), \tag{8a}$$

$$A=2\frac{[E_{mh}(E_D-iE_0)-E_{me}(E_D+iE_0)]}{E_{me}(E_D+iE_0)+E_{mh}(E_D-iE_0)+E_D^2+E_0^2}, \tag{8b}$$

$$B=2\frac{(E_{me}+E_{mh}+E_D)E_q}{E_{me}(E_D+iE_0)+E_{mh}(E_D-iE_0)+E_D^2+E_0^2}, \tag{8c}$$

with $E_q=eN_r/\epsilon\epsilon_0K$ being another characteristic field. In many practical cases, such as the GaAs/Al_xGa_{1-x}As MQW considered in this work, $\mu_h\ll\mu_e$ and so $E_{mh}\gg E_{me}$, leading to a marked simplification of the above expressions. For $E_D\ll E_0$, one may write

$$A\simeq 2\frac{E_{mh}}{E_{mh}+iE_0}, \tag{9a}$$

$$B \simeq 2\frac{(E_{mh}+E_D)E_q}{E_0^2 - iE_{mh}E_0}. \tag{9b}$$

The parameter Γ_{eh} determines the edge effects to be observed. It has a rather complex expression in terms of the characteristic fields for electrons and holes.

In order to determine the fields, one has to use appropriate boundary conditions at the MQW-buffer interfaces. The assumption that $j_z = 0$, implies that the MQW faces are free of charge. The boundary conditions are, therefore, the continuity of the parallel component of the electric field and of the perpendicular component of the displacement vector at the buffer-MQW boundaries. Under these conditions, the solution for the amplitude of the modulated transverse field can be written as

$$E_{x1} = E_{x1}^{(1D)}[1 - \delta(z)], \tag{10}$$

where $E_{x1}^{(1D)}$ stands for the one-dimensional solution and is given by

$$E_{x1}^{(1D)} = imE_q\frac{AK^2}{\Gamma_{eh}^2}, \tag{11}$$

and

$$\delta(z) = \frac{\cosh\Gamma_{eh}z}{(\epsilon_r\Gamma_{eh}/K)\sinh\Gamma_{eh}L/2 + \cosh\Gamma_{eh}L/2}, \tag{12}$$

ϵ_r being the ratio between the dielectric constants inside the photorefractive slab and outside (buffer layers). The function $\delta(z)$ measures the deviation of the two-dimensional solution with regard to the one-dimensional one. Its relative importance at the slab edges ($z = \pm L/2$) is

$$\delta(\pm L/2) = \frac{E_{x1}^{(1D)} - E_{x1}^{(2D)}(\pm L/2)}{E_{x1}^{(1D)}}$$

$$= \frac{1}{1 + (\epsilon_r\Gamma_{eh}/K)\tanh\Gamma_{eh}L/2}, \tag{13}$$

where 2D refers to the two-dimensional solution. Usually $(\epsilon_r\Gamma_{eh}/K)\tanh\Gamma_{eh}L/2 \gg 1$ and then

$$\delta(\pm L/2) \propto \frac{1}{\epsilon_r}, \tag{14}$$

i.e., the magnitude of the deviation is inversely dependent on ϵ_r. In other words, buffer layers with a high dielectric constant increase the effect. Then, the two-dimensional parallel field grating may be interpreted as the superposition of two grating components $E_x^{(1D)}$ and E_x':

$$E_x^{(1D)} = E_{x1}^{(1D)}e^{iKx}, \tag{15a}$$

$$E_x' = E_{x1}^{(1D)}\delta(z)e^{iKx}, \tag{15b}$$

which are, in general, phase-shifted an angle Φ given by

$$\Phi = \arctan\delta(z). \tag{16}$$

On the other hand, the amplitude of the modulated perpendicular field component can be obtained from Eq. (1e) as follows:

$$E_{z1} = mE_q\frac{AK}{\Gamma_{eh}}\left[\frac{\sinh\Gamma_{eh}z}{(\epsilon_r\Gamma_{eh}/K)\sinh\Gamma_{eh}L/2 + \cosh\Gamma_{eh}L/2}\right]$$

$$= E_{x1}^{(1D)}i\frac{\Gamma_{eh}}{K}\delta(z)\tanh\Gamma_{eh}z. \tag{17}$$

The ratio of the transverse to the longitudinal field amplitudes is

$$\frac{E_{z1}}{E_{x1}} = i\frac{\Gamma_{eh}}{K}\frac{\sinh\Gamma_{eh}z}{\cosh\Gamma_{eh}L/2 + (\epsilon_r\Gamma_{eh}/K)\sinh\Gamma_{eh}L/2 - \cosh\Gamma_{eh}z}. \tag{18}$$

At the edges ($z = \pm L/2$), this ratio reaches a maximum value given by

$$\frac{E_{z1}(\pm L/2)}{E_{x1}(\pm L/2)} = \frac{i}{\epsilon_r}, \tag{19}$$

indicating that the relative contribution of the longitudinal field decreases on increasing ϵ_r.

In summary, the effects derived from the finite thickness of the structure, i.e., from the two-dimensional solution, are, referring to the field:

(a) Departure of the parallel field E_{x1} from the one-dimensional value $E_{x1}^{(1D)}$ corresponding to an infinitely thick medium; (b) occurrence of a perpendicular field, E_{z1}, not predicted by the one-dimensional solution; (c) Non-flat (z-dependent) longitudinal profiles for both E_{x1} and E_{z1}.

The charge density also presents a departure from the one-dimensional solution and a nonflat profile as can be deduced from Eq. (5).

All these effects, generically designated as edge effects, are intimately related and determined by the single parameter Γ_{eh} which depends on Λ, the material parameters, and the applied field. It is related to the curvature of the transverse field profiles at $z = 0$ and to the slope of the longitudinal field profile. In other words, it measures the abruptness of the edge effects.

It is worthwhile noticing that the two-dimensional features (a) and (c) are enhanced by using buffer layers with ϵ_2 closer to or higher than ϵ_1. However, under these conditions, Γ_{eh} increases and the field profile becomes less curved. Finally, from expression (19) it is important to note that E_{x1} and E_{z1} are always $\pi/2$ phase shifted at the boundary.

B. Results

The above theoretical analysis is now applied to a photorefractive MQW structure of GaAs/$Al_xGa_{1-x}As$ using the parameters of Table I. First, a plot showing the dependence of Γ_{eh} on E_0 and Λ is given in Fig. 3(a). Γ_{eh} rapidly decreases on increasing E_0 and Λ and reaches a constant value for $E_0 \sim 6$ kV/cm and $\Lambda \sim 20$ μm. Except when explicitly indicated, all results presented next correspond to a MQW thickness of $L = 1$ μm, $\Lambda = 10$ μm, and $E_0 = 10$ kV/cm. Then, the longitudinal profiles for the modulated space-charge fields (E_{x1} and E_{z1}) and donor density N_{D1}^+ are, respectively, shown in Figs. 4 and 5. In order to illustrate the role of ϵ_r, two cases corresponding to $\epsilon_r = 12.25$ (Fig. 4) and $\epsilon_r = 3$ (Fig. 5) have been plotted. The first value corresponds to the absence of any buffer layer, whereas the second one would

TABLE I. Material parameters of a GaAs/Al_xGa_{1-x}As MQW structure.

Electron parallel mobility	μ_e	5000 $cm^2\ V^{-1}\ s^{-1}$
Hole parallel mobility	μ_h	300 $cm^2\ V^{-1}\ s^{-1}$
Recombination coefficient	γ	$5\times10^{-14}\ m^3\ s^{-1}$
Relative density of traps	N_r	$10^{17}\ cm^{-3}$
Relative permeability	ϵ_1	12.25
MQW thickness	L	1 μm

be obtained by using epoxy buffer layers ($\epsilon_2 \simeq 3.5$). The predictions of the one-dimensional model for the saturation values of N_{D1}^+ and E_{x1} are also included for comparison.

The main results are as follows.

(a) The parallel field E_{x1} shows an essentially flat profile. This field differs appreciably from that for an unbound medium even for $\epsilon_r = 12.25$. For $\epsilon_r = 3$, this deviation reaches a value over 20%. On the other hand, the phase mismatch of E_x with regard to the light pattern is in both cases essentially similar to that corresponding to the one-dimensional solution.

(b) The occurrence of a perpendicular field is a peculiar feature of the two-dimensional solution. The field is zero at the center of the slab and increases towards the MQW surfaces. For $\epsilon_r = 12.25$ it amounts to less than 10% of the parallel field. However, it reaches values $E_{z1} \simeq E_{x1}/3$ for $\epsilon_r = 3$. Under these conditions, the effect of the perpendicular field (e.g., on light diffraction) may become comparable to the parallel field and should be taken into account in any reliable model of MQW performance.

(c) Edge effects are quite important for N_{D1}^+ that reaches values near the film faces which are close to twice those of the one-dimensional solution. An appreciable ($\simeq 10\%$) accumulation of charge is also observed for $\epsilon_r = 3$.

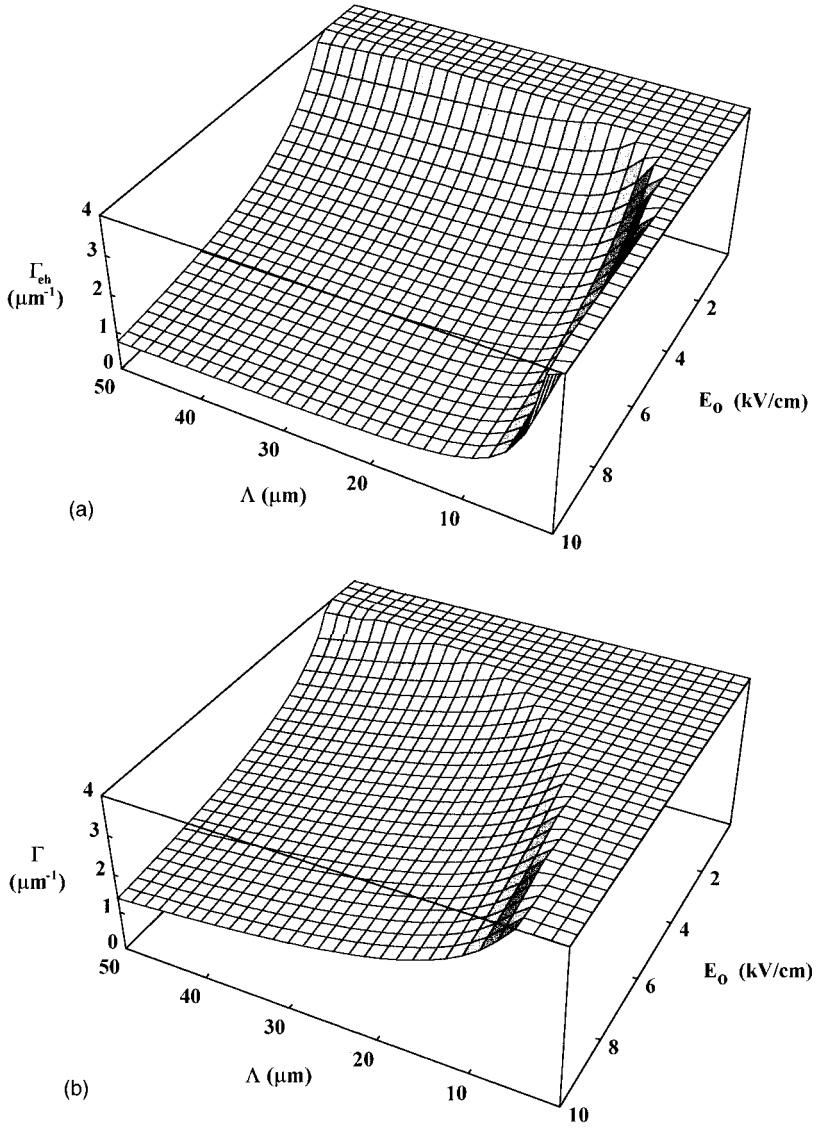

FIG. 3. (a) Γ_{eh} and (b) Γ as a function of E_0 and Λ.

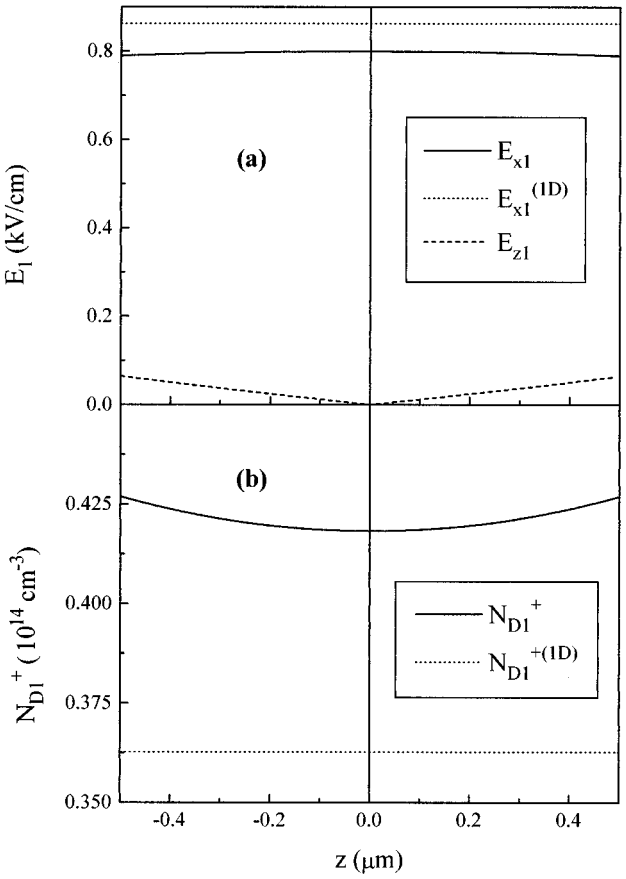

FIG. 4. Longitudinal profiles for the modulated amplitude of (a) the space-charge fields and (b) the trap densities. $E_0=10$ kV/cm, $\Lambda=10$ μm, $\epsilon_r=12.25$ and carrier generation from interband transitions.

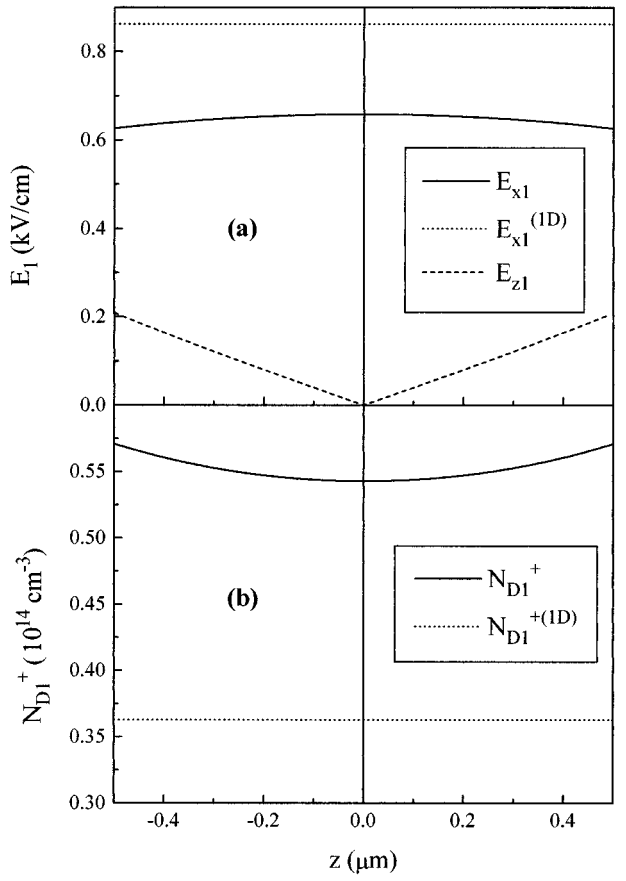

FIG. 5. Longitudinal profiles for the modulated amplitude of (a) the fields and (b) the trap densities. $E_0=10$ kV/cm, $\Lambda=10$ μm, $\epsilon_r=3$ and carrier generation from interband transitions.

C. Dependence on physical parameters

In order for the effects to stand out all simulations have been carried out for the case $\epsilon_r=3$. The dependence of the field amplitudes E_{x1} and E_{z1} at the edges on the ratio Λ/L are illustrated in Fig. 6(a). The one-dimensional solution for E_{x1} is also shown for comparison. We find pronounced edge effects which are relevant even for long periods $\Lambda>25$ μm. On the other hand, the relative magnitude E_{z1}/E_{x1} of the perpendicular field does not essentially depend on the film thickness and reaches the value $1/\epsilon_r$ at the MQW boundaries. As a consequence of the relatively large contribution of the perpendicular field and its $\sim\pi/2$ mismatch with regard to E_{x1}, a significant modification of the overall phase mismatch between the light-induced refractive index grating and the light intensity pattern may appear. In fact, high coupling gains associated to enhanced phase-mismatch have been measured in some experimental work.[22] Although they have been satisfactorily explained due to electron velocity saturation at high fields,[11,23] some additional contribution associated to the simultaneous presence of the $\pi/2$-shifted parallel and perpendicular fields cannot be disregarded in the quasisteady range of times.

Finally, Fig. 6(b) shows the dependence of E_{x1}, and E_{z1} at the MQW boundaries on the applied parallel field E_0 for $\Lambda=10$ μm. The deviation between the one- and two-dimensional formulations clearly depend on E_0 and the edge effects become quite appreciable for $E_0\gtrsim 2$ kV/cm. The two-dimensional curve saturates for lower E_0 than the one-dimensional one. This seems to be in accordance with experimental data by Wang *et al.*[22] that show a saturation of the parallel field E_{x1} at $E_0<5$ kV/cm. One should mention that this saturation behavior can also be predicted from a one-dimensional model that takes into account electron velocity saturation.[11]

IV. COMPARISON WITH THE SHORT-TIME SOLUTION

It is interesting to compare the above results for the quasisteady regime with those corresponding to the initial recording stage. The short-time solution of Eqs. (1) for the MQW structure, has been obtained by extending the approach previously developed for an isotropic film with a single type of carrier.[18] One imposes first the pseudoequilibrium condition for electrons and holes carrier densities and assumes that the trap concentrations keep the initial values $N_D^0(0)$ and $N_D^+(0)$. Then, one follows essentially the same steps considered in Ref. 18. The two-dimensional short-time solution for the amplitude of the transverse field is

$$E_{x1}=E_{x1}^{(1D)ST}\left(1-\frac{\cosh Kz}{\cosh KL/2+(\epsilon_1/\epsilon_2)\sinh KL/2}\right), \tag{20}$$

where

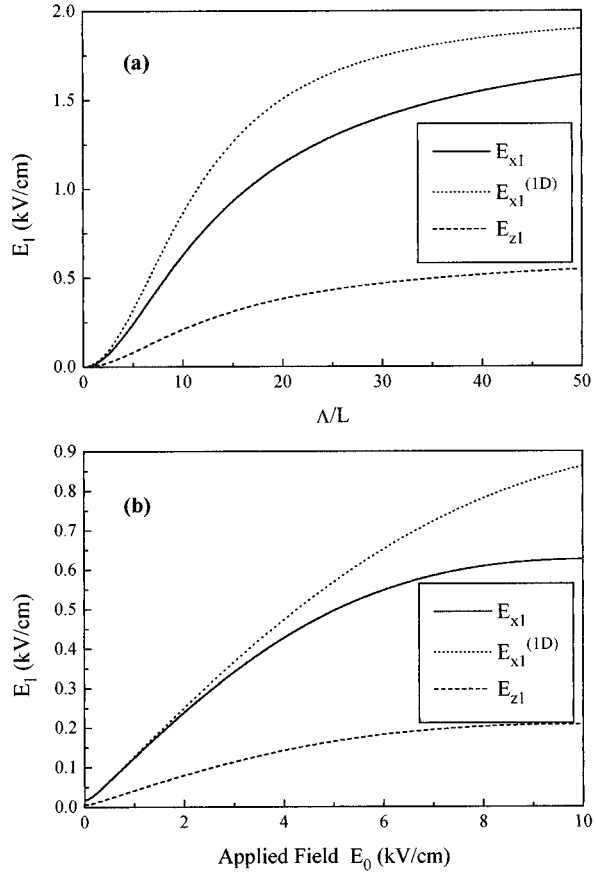

FIG. 6. Dependence of the amplitude of the space charge fields at the MQW boundaries on (a) Λ/L for $E_0=10$ kV/cm and (b) the applied field E_0 for $\Lambda=2$ μm. The relative permitivity is $\epsilon_r=3$, and carrier generation from interband transitions is assumed.

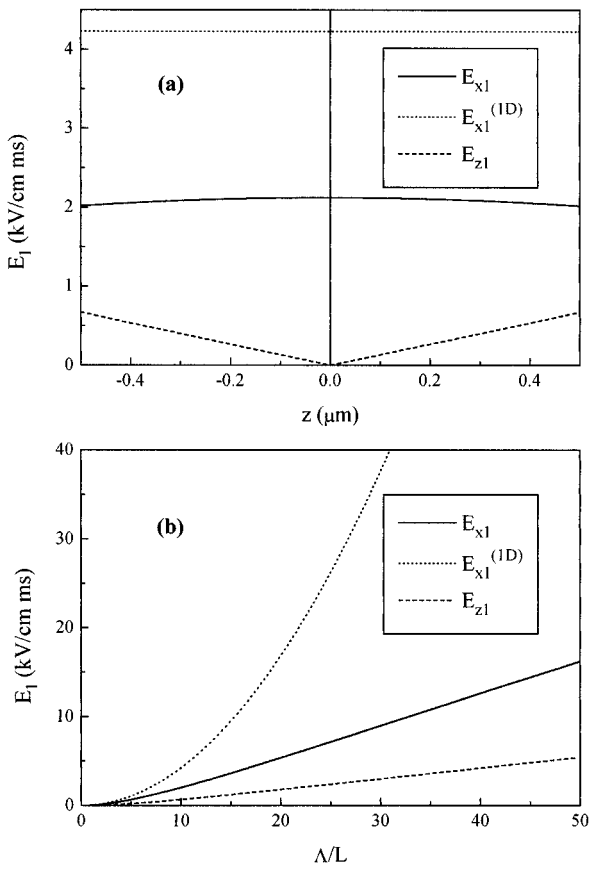

FIG. 7. (a) Longitudinal profile of the initial recording rate for the fields for $\Lambda=10$ μm. (b) Dependence of the initial recording rate for the fields on Λ/L. $E_0=10$ kV/cm, $\epsilon_r=3$, and carriers are generated from interband transitions.

$$E_{x1}^{(1D)ST}=mt\left(\frac{1}{\tau_{De}}\frac{2E_{me}(E_D-iE_0)}{2E_{me}+E_D-iE_0}+\frac{1}{\tau_{Dh}}\frac{2E_{mh}(E_D+iE_0)}{2E_{mh}-E_D+iE_0}\right) \tag{21}$$

is the one-dimensional short-time solution and $\tau_D=\epsilon_0\epsilon_1/(en\mu)$ is the dielectric relaxation time. One should note that Eq. (20) is identical to Eq. (10) provided that Γ_{eh} is replaced by K in the expression (12) for $\delta(z)$. The longitudinal field amplitude is immediately derived from Eq. (1e) as follows:

$$E_{z1}=iE_{x1}^{(1D)ST}\frac{\sinh Kz}{\cosh KL/2+(\epsilon_1/\epsilon_2)\sinh KL/2}. \tag{22}$$

The field profiles and Λ dependence are plotted in Figs. 7(a) and 7(b), respectively. The same parameters as those of Fig. 5 have been used. The edge effects for the fields and the departure from the one-dimensional solution are much more clearly increased here due to the substitution of Γ_{eh} by K. Consequently, as can be seen in Fig. 7(b), edge effects are enhanced on increasing Λ which is different from the quasisteady behavior. In conclusion, edge effects are very pronounced during the initial stages of recording but are progressively screened out when approaching the quasisteady situation.

V. CARRIER GENERATION FROM DONORS

Let us now briefly consider for comparison the physical situation depicted in Fig. 2(b). The two-dimensional equations describing the steady-state space-charge fields generated in the slab are a simple generalization of those initially put forward for the one-dimensional case, i.e., an unbound medium in the z direction.[10] They appear as follows:

$$\sigma IN_D-\gamma nN_A=0, \tag{23a}$$

$$\frac{\partial j_x}{\partial x}+\frac{\partial j_z}{\partial z}=0, \tag{23b}$$

$$\frac{\partial E_x}{\partial x}+\frac{\partial E_z}{\partial z}=\frac{\rho}{\epsilon\epsilon_0}, \tag{23c}$$

$$\frac{\partial E_x}{\partial z}-\frac{\partial E_z}{\partial x}=0. \tag{23d}$$

N_D and N_A are the donor and acceptor concentrations and the other symbols have the usual meaning. The light intensity pattern is assumed to have a modulation depth $m\ll 1$ to permit a linear approximation. Following the same steps as for case III, one obtains after some straightforward algebra

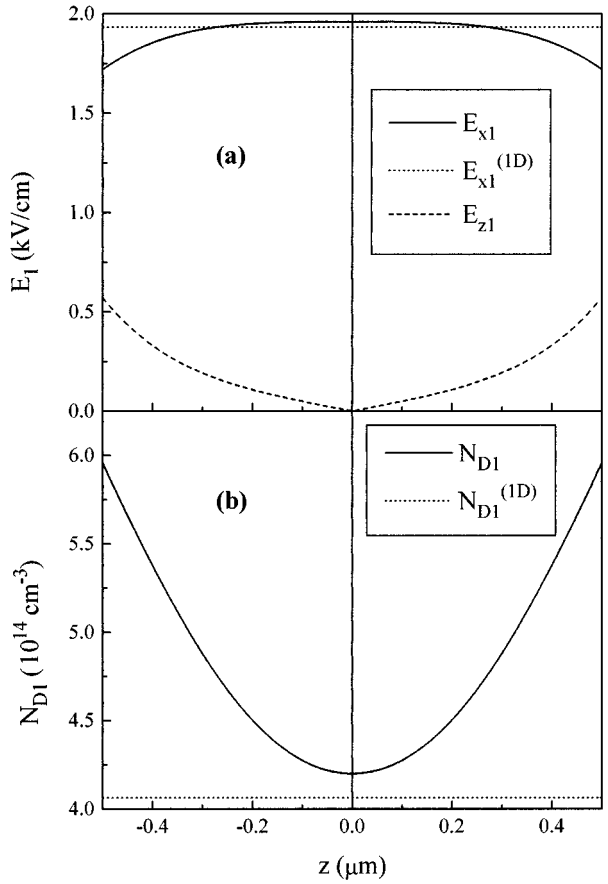

FIG. 8. Longitudinal profiles for the modulated amplitude of (a) the space-charge fields and (b) the trap densities. $E_0=10$ kV/cm, $\Lambda=2$ μm, $\epsilon_r=3$, and carrier generation from donors is assumed.

$$\frac{\partial^2 E_{x1}}{\partial z^2}-\Gamma^2 E_{x1}-imK^2E_q=0, \tag{24}$$

where

$$\Gamma^2=K^2\left(1+\frac{E_q}{E_D-iE_0}\right). \tag{25}$$

Equation (24) is essentially identical to Eq. (7) except for the absence of parameter A. Therefore all the results obtained in that section can be immediatly generalized to this case. The relevance of the edge effect is governed here by the parameter Γ whose dependence on E_0 and Λ is shown in Fig. 3(b) for comparison purposes. Values for Γ (Γ_{eh} in Sec. III) are quite similar for the two different physical cases. As an illustration Fig. 8 displays the field profiles for $\epsilon_r=3$. The comparison of this plot with that in Fig. 5 shows that edge effects are not essentially dependent on the operative photoionization mechanisms. In particular, large edge effects for the donor densities N_{D1} with important charge accumulation near the MQW boundaries are observed in this case.

VI. SUMMARY AND CONCLUSIONS

The results obtained in this paper show the need of a two-dimensional formulation to accurately describe the quasi-steady-state of the photorefractive effect in MQW heterostructures with low longitudinal mobility. The main effect associated to the small thickness of the structure is the occurrence of a perpendicular component of the field E_z that in some cases is comparable to the parallel field E_x. On the other hand, the E_x component differs from the value obtained from previous one-dimensional models. Moreover, both components have nonflat profiles. Finally, edge effects are also relevant for the trap density. In fact, charge accumulation regions near the MQW boundaries are predicted.

The dependence of these effects with different parameters (relative permitivity, applied field, and grating period) has been studied. Particularly important is the inverse dependence of the edge effects on the ratio between the MQW and buffer permitivities.

The situation for the quasi-steady-state contrasts with that for the short-time regime. There, more relevant edge effects are found for the field whereas the space-charge exhibits almost flat profiles. One should conclude that the initial edge effects are progressively ''screened out'' due to the creation of accumulation charge regions near the boundaries.

ACKNOWLEDGMENTS

This work has been carried out under the European contract No. CI1*−CT94−0039. One of us (M.A.) gratefully acknowledges the Spanish Ministerio de Educación y Ciencia for support.

*Electronic address: maria.aguilar@uam.es

[1] D. D. Nolte, MRS Bull. **1XX**, 44 (1994).
[2] D. D. Nolte and M. R. Melloch, in *Photorefractive Effects and Materials*, edited by D. D. Nolte (Kluwer, Boston, 1995), Chap. 7, pp. 374–451.
[3] S. Ducharme, J. C. Scott, R. J. Tweig, and W. E. Moerner, Phys. Rev. Lett. **66**, 1846 (1991).
[4] K. Meerholtz, B. L. Volodin, Sandalphon, B. Kippelen, and N. Peyghambarian, Nature (London) **371**, 497 (1994).
[5] A. Partovi, A. M. Glass, D. H. Olson, G. J. Zydzik, K. T. Short, R. D. Feldman, and R. F. Austin, Appl. Phys. Lett. **59**, 1832 (1991).
[6] A. Partovi, A. M. Glass, T. H. Chiu, and D. T. Liu, Opt. Lett. **18**, 906 (1993).
[7] A. Partovi, A. M. Glass, D. H. Olson, G. J. Zydzik, H. M. O'Bryan, T. H. Chiu, and W. H. Knox, Appl. Phys. Lett. **62**, 464 (1993).
[8] A. Partovi, Opt. Mat. **4**, 330 (1995).
[9] R. M. Brubaker, Q. N. Wang, D. D. Nolte, E. S. Harmon, and M. R. Melloch, J. Opt. Soc. Am. B **11**, 1038 (1994).
[10] N.V. Kukhtarev, V. B. Markov, S. G. Odulov, M. Soskin, and V. L. Vinetskii, Ferroelectrics **22**, 949 (1979).
[11] Q. N. Wang, R. M. Brubaker, and D. D. Nolte, J. Opt. Soc. Am. B **11**, 1773 (1994).
[12] L. F. Magaña, M. Carrascosa, and F. Agulló-López, J. Opt. Soc. Am. B **11**, 1651 (1994).
[13] D. C. Hutchings, C. B. Park, and A. Miller, Appl. Phys. Lett. **59**, 3009 (1991).
[14] D. Mahgerefteh and E. Garmire, Opt. Lett. **18**, 616 (1993).
[15] E. Canoglu, C. M. Yang, E. Garmire, D. Mahgerefteh, A. Partovi,

T. H. Chiu, and G. J. Zydzik, Appl. Phys. Lett. **69**, 316 (1996).
[16] S. L. Smith, L. Hesselink, and A. Partovi, Appl. Phys. Lett. **66**, 3117 (1996).
[17] S. L. Smith and L. Hesselink, J. Opt. Soc. Am. B **11**, 1878 (1994).
[18] M. Aguilar, M. Carrascosa, F. Agulló-López, and L. F. Magaña, J. Appl. Phys. **78**, 4840 (1995).
[19] F. Agulló-López, M. Aguilar, and M. Carrascosa, Pure Appl. Opt. **5**, 495 (1996).
[20] M. Aguilar, M. Carrascosa, F. Agulló-López, L. F. Magaña, and L. Solymar, J. Opt. Soc. Am. B **13**, 2630 (1996).
[21] L. Solymar, M. Aguilar, and F. Agulló-López, J. Appl. Phys. **80**, 1268 (1996).
[22] Q. N. Wang, R. M. Brubaker, D. D. Nolte, and M. R. Melloch, J. Opt. Soc. Am. B **9**, 1626 (1992).
[23] Q. N. Wang, R. M. Brubaker, and D. D. Nolte, Opt. Lett. **19**, 822 (1994).